Engineering Transactions, **67**(1): 3–19, 2019, doi: 10.24423/EngTrans.820.20190308
Polish Academy of Sciences • Institute of Fundamental Technological Research (IPPT PAN)
Université de Lorraine • Poznan University of Technology

Research Paper

Cross-diffusion Effects on MHD Mixed Convection over a Stretching Surface in a Porous Medium with Chemical Reaction and Convective Condition

Marimuthu BHUVANESWARI[1)], Sheniyappan ESWARAMOORTHI[2)]
Sivanandam SIVASANKARAN[3)], Ahmed Kadhim HUSSEIN[4)]

[1)] *Department of Mathematics*
Kongunadu Polytechnic College, D.Gudalur
Dindigul 624 620, Tamil Nadu, India

[2)] *Department of Mathematics*
Dr.NGP Arts & Science College
Coimbatore 641048, Tamil Nadu, India

[3)] *Department of Mathematics, King Abdulaziz University*
Jeddah 21589, Saudi Arabia
e-mail: sd.siva@yahoo.com

[4)] *Department of Mechanical Engineering, Babylon University*
Babylon City, Iraq

In this paper, we investigate the Dufour and Soret effects on MHD mixed convection of a chemically reacting fluid over a stretching surface in a porous medium with convective boundary condition. The similarity transformation is used to reduce the governing non-linear partial differential equations into ordinary differential equations. Then, they are solved analytically by using the homotopy analysis method (HAM) and are solved numerically by the Runge-Kutta fourth-order method. The analytical and numerical results for the velocity, temperature, concentration, skin friction, Nusselt number and Sherwood number are discussed.

Key words: mixed convection; viscoelastic fluid; Dufour/Soret effect; magnetic field; chemical reaction.

1. Introduction

Combined heat and mass transfer with magnetic field has gained considerable attention due to its vast applications in many fields such as geothermal reservoirs, thermal insulation, MHD generator, plasma studies, liquid metals fluid, power generation system, etc. MHD boundary layer flow, heat and mass transfer over a vertical surface in a porous medium with Soret and Dufour effects were numerically studied by Postelnicu [1]. He found that the hydrodynamic boundary layer thickness increases on increasing the magnetic field parameter. Abel and Mahesha [2] investigated the problem of MHD boundary layer flow of a viscoelastic fluid. They found that the transverse magnetic field contributes to the thickening of the thermal boundary layer. The study of MHD boundary layer flow over a stretching surface was done by several investigators, see [3–12].

Boundary layer flow with internal heat generation or absorption past a stretching surface has received considerable attention because of its many practical applications such as, heat removal from nuclear fuel debris, underground disposal of radioactive waste material, storage of food items, cooling of nuclear reactors, electronic chips and semiconductor wafers. The Lie group analysis of natural convection heat and mass transfer over a semi-infinite inclined surface with heat generation or absorption was numerically investigated by Bhuvaneswari *et al.* [13]. They found that the local Nusselt number decreases on increasing the heat generation or absorption parameter. Numerous researchers have discussed the heat generation effect on boundary layer flow with different fluids, see Chamkha and Ahmed [14], Karthikeyan *et al.* [15], and Kasmani *et al.* [16].

The study of boundary layer flow concerning convective boundary condition plays an important role in several engineering and industrial processes such as transpiration cooling and material drying. Hydromagnetic mixed convection with heat and mass transfer past a vertical plate embedded in a porous medium with convective boundary condition was numerically studied by Makinde [17]. They found that the thermal boundary thickness increases with increasing the Biot number. The convective boundary condition over a stretching surface has been considered by some researchers [18–22].

Hence, based on the above discussion, the purpose of the present study is to extend the work of Hayat *et al.* [23] to include a magnetic field, heat generation or absorption, chemical reaction and convective boundary condition.

2. Mathematical formulation

We consider the heat and mass transfer effects in a mixed convection boundary layer flow past a vertical stretching surface in a porous medium filled with a viscoelastic fluid. A uniform magnetic field of strength B_o is applied. The Soret and Dufour effects are included to study the heat and mass transfer. The following assumptions are made in the study. The induced magnetic field is neglected for small magnetic Reynolds number. The fluid phase is assumed to be heat generating or absorbing. The first order homogeneous chemical reaction is taking place in the flow. The porous medium is isotropic and in thermodynamic equilibrium with local fluid. It is also assumed that viscous dissipation and Joule heating are neglected in the study.

Under these assumptions along with the Boussinesq approximation, the governing equations of the mass, momentum, energy and concentration boundary layers are given by

$$\frac{\partial u}{\partial x} + \frac{\partial v}{\partial y} = 0, \tag{2.1}$$

$$u\frac{\partial u}{\partial x} + v\frac{\partial u}{\partial y} = \nu\frac{\partial^2 u}{\partial y^2} + k_0\left(u\frac{\partial^3 u}{\partial x \partial y^2} + \frac{\partial u}{\partial x}\frac{\partial^2 u}{\partial y^2} + \frac{\partial u}{\partial y}\frac{\partial^2 v}{\partial y^2} + v\frac{\partial^3 u}{\partial y^3}\right) - \frac{\nu}{k_1}u + g[\beta_T(T - T_\infty) + \beta_C(C - C_\infty)] - \frac{\sigma B_0^2}{\rho}u, \tag{2.2}$$

$$u\frac{\partial T}{\partial x} + v\frac{\partial T}{\partial y} = \alpha_m\frac{\partial^2 T}{\partial y^2} + \frac{D_e k_T}{c_s c_p}\frac{\partial^2 C}{\partial y^2} + \frac{Q}{\rho c_p}(T - T_\infty), \tag{2.3}$$

$$u\frac{\partial C}{\partial x} + v\frac{\partial C}{\partial y} = D_e\frac{\partial^2 C}{\partial y^2} + \frac{D_e k_T}{T_m}\frac{\partial^2 T}{\partial y^2} - k_2(C - C_\infty), \tag{2.4}$$

where u and v are the velocity components, x and y are the space coordinates, ν is the kinematic viscosity, k_0 is the viscoelastic parameter, k_1 is the permeability of the porous medium, g is the acceleration due to gravity, β_T is the coefficient of thermal expansion, β_C is the coefficient of concentration expansion, σ is the electrical conductivity of the fluid, ρ is the density of the fluid, T is the temperature of the fluid, α_m is the thermal diffusivity, D_e is the mass diffusivity, k_T is the thermal diffusion ratio, c_s is the free stream concentration, c_p is the specific heat, Q is the internal heat generation (> 0) or absorption (< 0) of the fluid, C is the concentration of the fluid, T_m is the mean fluid temperature and k_2 is the coefficient of chemical reaction.

The boundary conditions can be expressed as,

$$\begin{gathered} u = U_w(x) = ax, \qquad v = 0, \qquad -k\frac{\partial T}{\partial y} = h_f(T_f - T), \\ C = C_w(x) = C_\infty + cx \qquad \text{at} \quad y = 0, \\ u \to 0, \qquad \frac{\partial u}{\partial y} \to 0, \qquad T \to T_\infty, \qquad C \to C_\infty \qquad \text{as} \quad y \to \infty, \end{gathered} \tag{2.5}$$

where a and c are the positive constants, k is the thermal conductivity of the fluid, h_f is the heat transfer coefficient and T_f is the temperature of the hot fluid.

Now, the following dimensionless variables are introduced:

$$\eta = \sqrt{\frac{a}{\nu}}y, \qquad u = axf'(\eta), \qquad v = -\sqrt{a\nu}f(\eta),$$
$$\theta(\eta) = \frac{T - T_\infty}{T_f - T_\infty}, \qquad \phi(\eta) = \frac{C - C_\infty}{C_w - C_\infty}. \tag{2.6}$$

By using Eq. (2.6), and Eqs (2.2)–(2.4) can be reduced to the following ordinary differential equations:

$$f''' + ff'' - f'^2 + K(2f'f''' - f''^2 - ff^{iv}) - (\mathrm{Ha}^2 + \gamma)f' + \mathrm{Ri}(\theta + N\phi) = 0, \tag{2.7}$$
$$\theta'' + \Pr(f\theta' - \theta f') + \Pr H_g\,\theta + \Pr \mathrm{Du}\,\phi'' = 0, \tag{2.8}$$
$$\phi'' + \Pr \mathrm{Le}(f\phi' - \phi f') - \Pr \mathrm{Le}\, C_r\phi + \mathrm{Sr}\,\mathrm{Le}\,\theta'' = 0. \tag{2.9}$$

Boundary conditions (2.5) in terms of f, θ and ϕ, becomes,

$$f(0) = 0, \qquad f'(0) = 1, \qquad \theta'(0) = -\mathrm{Bi}[1 - \theta(0)], \qquad \phi(0) = 1,$$
$$f'(\infty) = 0, \qquad f''(\infty) = 0, \qquad \theta(\infty) = 0, \qquad \phi(\infty) = 0, \tag{2.10}$$

where $K = \frac{k_0 a}{\nu}$ is the viscoelastic parameter, $\mathrm{Ha}^2 = \frac{\sigma B_0^2}{\rho a}$ is the Hartmann number, $\gamma = \frac{\nu}{ak_1}$ is the constant dimensionless porosity parameter, $\mathrm{Ri} = \frac{\mathrm{Gr}}{\mathrm{Re}^2}$ is the Richardson number with $\mathrm{Gr} = \frac{g\beta_T(T_f - T_\infty)x^3}{\nu^2}$ is the local Grashof number and $\mathrm{Re} = \frac{U_w x}{\nu}$ is local Reynolds number, $N = \frac{\beta_c}{\beta_T}\frac{(C_w - C_\infty)}{(T_f - T_\infty)}$ is the buoyancy ratio parameter, $\Pr = \frac{\nu}{\alpha_m}$ is the Prandtl number, $H_g = \frac{Q}{\rho c_p a}$ is the internal heat generation/absorption parameter, $\mathrm{Du} = \frac{D_e k_T}{c_s c_p \nu}\frac{(C_w - C_\infty)}{(T_f - T_\infty)}$ is the Dufour number, $\mathrm{Le} = \frac{\alpha_m}{D_e}$ is the Lewis number, $C_r = \frac{k_2}{a}$ is dimensionless chemical reaction parameter, $\mathrm{Sr} = \frac{D_e k_T}{T_m \alpha_m}\frac{(T_f - T_\infty)}{(C_w - C_\infty)}$ is the Soret number, and $\mathrm{Bi} = \frac{h_f\sqrt{\frac{\nu}{a}}}{k}$ is the Biot number.

The skin friction coefficient, local Nusselt number, and the local Sherwood number are important physical parameters. These can be obtained from the following expressions:

$$C_f = \frac{\tau_w}{\rho U_w^2/2}, \qquad \mathrm{Nu} = \frac{xq_w}{k(T_f - T_\infty)}, \qquad \text{and} \qquad \mathrm{Sh} = \frac{xj_w}{D_e(C_w - C_\infty)},$$

where

$$\tau_w = \mu \left(\frac{\partial u}{\partial y}\right)_{y=0} + k_0 \left(u\frac{\partial^2 u}{\partial x \partial y} + v\frac{\partial^2 u}{\partial y^2} - 2\frac{\partial v}{\partial y}\frac{\partial u}{\partial y}\right)_{y=0} \quad \text{is the wall shear stress,}$$

$$q_w = -k\left(\frac{\partial T}{\partial y}\right)_{y=0} \quad \text{is the surface heat flux, and}$$

$$j_w = -k\left(\frac{\partial C}{\partial y}\right)_{y=0} \quad \text{is the surface mass flux.}$$

Then the reduced skin friction coefficient, local Nusselt number, and local Sherwood number are given by

$$\frac{1}{2}C_f\mathrm{Re}^{1/2} = (1+3K)f''(0), \quad \mathrm{Nu}/\mathrm{Re}^{1/2} = -\theta'(0), \quad \text{and} \quad \mathrm{Sh}/\mathrm{Re}^{1/2} = -\phi'(0).$$

3. Solutions

3.1. Analytical solution

The non-linear boundary layer equations (2.7)–(2.9) with boundary conditions (2.10) are solved analytically using homotopy analysis method. The explicit formulae for $f''(\eta)$, $\theta'(\eta)$ and $\phi'(\eta)$ are expressed by the set of base functions, see Hayat *el al.* [23]. We take the initial guesses as $f_0(\eta) = 1 - e^{-\eta}$, $\theta_0(\eta) = \frac{\mathrm{Bi}\, e^{-\eta}}{1+\mathrm{Bi}}$ and $\phi_0(\eta) = e^{-\eta}$. After substituting the m-th order deformation equations, the resulting equations are solved using HAM with 15th order approximations. These solutions contain auxiliary parameters h_f, h_θ and h_ϕ, which have a key role in adjusting and controlling the convergence of the solutions. The h_f, h_θ and h_ϕ curves are displayed in Fig. 1. It is observed that the ranges for admissible values of h_f, h_θ and h_ϕ are $-0.8 \leq h_f,\ h_\theta \leq -0.25$ and $-0.95 \leq h_\phi \leq -0.1$, respec-

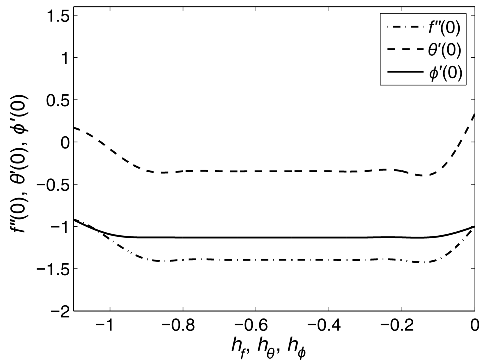

Fig. 1. h curves of $f''(0)$, $\theta'(0)$ and $\phi'(0)$ with $K = 0.1$, $\mathrm{Ha}^2 = 0.1$, $\gamma = 1.0$, $\mathrm{Ri} = 1.0$, $N = -0.5$, $\mathrm{Pr} = 0.7$, $\mathrm{Le} = 1.0$, $H_g = -0.5$, $\mathrm{Du} = 0.1$, $\mathrm{Bi} = 0.5$, $C_r = 1.0$, and $\mathrm{Sr} = 0.2$.

tively. It is found from our computation that the series solution convergence is in the whole region of η when $h_f = h_\theta = h_\phi = -0.6$.

3.2. Numerical solution

The system of transformed equations (2.7)–(2.9) with boundary conditions (2.10) is numerically solved by employing a Runge-Kutta method with initial guessing $f''(0)$, $\theta'(0)$ and $\phi'(0)$. This process is continued until we obtain the desired accuracy (10^{-6}). The analytical and numerical results are compared in Tables 2–4. This comparison proves the accuracy of our analytical and numerical results.

4. Results and discussion

In this section, a representative set of graphical results for the velocity ($f'(\eta)$), temperature ($\theta(\eta)$) and concentration ($\phi(\eta)$) as well as the skin friction coefficient $\left(\frac{1}{2}C_f \,\mathrm{Re}^{1/2}\right)$, the local Nusselt number $\left(\mathrm{Nu}/\mathrm{Re}^{1/2}\right)$ and the local Sherwood number $\left(\mathrm{Sh}/\mathrm{Re}^{1/2}\right)$ are presented and discussed for various parameters, such as viscoelastic parameter (K), Hartmann number (Ha^2), porosity parameter (γ), Richardson number (Ri), buoyancy ratio parameter (N), internal heat generation or absorption parameter (H_g), Dufour number (Du), chemical reaction parameter (C_r), Soret number (Sr) and Biot number (Bi) with the fixed values of Prandtl number ($\mathrm{Pr} = 0.054$) and Lewis number ($\mathrm{Le} = 1.0$).

Table 1 presents the comparison of $f''(0)$ between our results and published results. It is observed from the table that the results are in good agreement. Table 2 shows the local skin friction for different values of K, γ, Ri, N, Du, Bi, and Sr. It is observed that the local skin friction increases with increasing the values of Ri, N, Du and Bi and it decreases with increasing the values of K, γ and Sr. The local Nusselt number for different values of K, γ, Ri, N, Du, Bi, and Sr are presented in Table 3. It is found that the surface heat transfer rate

Table 1. Comparison of $f''(0)$ for various values of porosity parameter (γ) when $K = \mathrm{Ri} = \mathrm{Ha}^2 = 0$.

γ	$f''(0)$		
	HAM	Numerical	Hayat *et al.* [23]
0.0	1.000000	1.000000	1.000000
0.5	1.224745	1.224750	1.224747
1.0	1.414214	1.414251	1.414217
1.5	1.581139	1.581142	1.581147
2.0	1.732038	1.732059	1.732057

Table 2. Local skin friction for different values of K, γ, Ri, N, Du, Bi, and Sr.

K	γ	Ri	N	Du	Bi	Sr	C_f HAM	C_f Numerical	C_f Error [%]
0.00	0.50	1.0	−0.5	0.1	0.5	0.2	−1.247856	−1.248011	0.01
0.25							−1.952824	−1.952059	0.04
0.50							−2.546753	−2.547615	0.03
0.75							−3.065881	−3.066012	0.00
1.00							−3.531064	−3.531064	0.00
0.10	0.00	1.0	−0.5	0.1	0.5	0.2	−1.280326	−1.280654	0.03
	0.25						−1.419095	−1.4189727	0.01
	0.50						−1.546555	−1.546022	0.04
	0.75						−1.664906	−1.6648935	0.00
	1.00						−1.775740	−1.775006	0.04
0.10	0.50	0.0	−0.5	0.1	0.5	0.2	−1.567859	−1.568002	0.01
		3.0					−1.494197	−1.494223	0.00
		5.0					−1.425791	−1.425837	0.00
		8.0					−1.281449	−1.281473	0.00
		10.0					−1.145862	−1.145990	0.01
0.10	0.50	1.0	−2.0	0.1	0.5	0.2	−3.625070	−3.625294	0.01
			−1.0				−2.056629	−2.056703	0.00
			0.0				−1.124619	−1.124901	0.03
			1.0				−0.417227	−0.418524	0.31
			2.0				0.195274	0.195462	0.10
0.10	0.50	1.0	−0.5	0.0	0.5	0.2	−1.548106	−1.548057	0.00
				0.5			−1.540301	−1.540753	0.03
				1.0			−1.532411	−1.532618	0.01
				1.5			−1.524407	−1.524951	0.04
				2.0			−1.516297	−1.516842	0.04
0.10	0.50	1.0	−0.5	0.1	0.1	0.2	−1.916161	−1.916102	0.00
					0.5		−1.546555	−1.546673	0.01
					1.0		−1.321212	−1.321439	0.02
					3.0		−1.016074	−1.016249	0.02
					5.0		−0.921386	−0.921577	0.02
					10.0		−0.837851	−0.837946	0.01
0.10	0.50	1.0	−0.5	0.1	0.5	0.0	−1.538820	−1.538884	0.00
						0.5	−1.558396	−1.558654	0.02
						1.0	−1.578786	−1.578348	0.03
						1.5	−1.600025	−1.600917	0.06
						2.0	−1.622146	−1.622668	0.03

increases as the K, Bi, and Sr are increasing and it decreases with increasing the values of γ, Ri, and Du. It is observed from the Table 4 that the surface mass

Table 3. Local Nusselt number for different values of K, γ, Ri, N, Du, Bi, and Sr.

K	γ	Ri	N	Du	Bi	Sr	Nu		
							HAM	Numerical	Error [%]
0.00	0.50	1.0	−0.5	0.1	0.5	0.2	0.157016	0.157369	0.22
0.25							0.158768	0.158654	0.07
0.50							0.160240	0.160334	0.06
0.75							0.161496	0.161741	0.15
1.00							0.162580	0.162829	0.15
0.10	0.00	1.0	−0.5	0.1	0.5	0.2	0.161088	0.161114	0.02
	0.25						0.159197	0.159618	0.27
	0.50						0.157756	0.157994	0.15
	0.75						0.156597	0.156705	0.07
	1.00						0.155627	0.155749	0.08
0.10	0.50	0.0	−0.5	0.1	0.5	0.2	0.158284	0.158093	0.12
		3.0					0.156625	0.156833	0.13
		5.0					0.155420	0.155607	0.12
		8.0					0.153644	0.153722	0.05
		10.0					0.152690	0.152950	0.17
0.10	0.50	1.0	−2.0	0.1	0.5	0.2	0.201667	0.201811	0.07
			−1.0				0.160881	0.161002	0.08
			0.0				0.158389	0.158501	0.07
			1.0				0.162127	0.162252	0.08
			2.0				0.165588	0.165692	0.06
0.10	0.50	1.0	−0.5	0.0	0.5	0.2	0.158628	0.158816	0.12
				0.5			0.154301	0.154498	0.13
				1.0			0.150059	0.150244	0.12
				1.5			0.145900	0.146011	0.08
				2.0			0.141826	0.141957	0.09
0.10	0.50	1.0	−0.5	0.1	0.1	0.2	0.042614	0.042598	0.04
					0.5		0.157756	0.157906	0.10
					1.0		0.237170	0.237323	0.06
					3.0		0.358019	0.358288	0.08
					5.0		0.398877	0.398995	0.03
					10.0		0.436282	0.436506	0.05
0.10	0.50	1.0	−0.5	0.1	0.5	0.0	0.156947	0.157002	0.04
						0.5	0.159015	0.159285	0.17
						1.0	0.161237	0.161397	0.10
						1.5	0.163616	0.163808	0.12
						2.0	0.166160	0.166328	0.10

transfer rate increases with increasing of the values of K, N, and Du. On the other hand, it is a decreasing function of γ, Ri, Bi, and Sr.

Table 4. Local Sherwood number for different values of K, γ, Ri, N, Du, Bi, and Sr.

K	γ	Ri	N	Du	Bi	Sr	Sh		
							HAM	Numerical	Error [%]
0.00	0.50	1.0	−0.5	0.1	0.5	0.2	0.298076	0.298341	0.09
0.25							0.300916	0.301035	0.04
0.50							0.303303	0.303513	0.07
0.75							0.305360	0.305586	0.07
1.00							0.307162	0.307319	0.05
0.10	0.00	1.0	−0.5	0.1	0.5	0.2	0.303721	0.303977	0.08
	0.25						0.301302	0.301593	0.10
	0.50						0.299277	0.299403	0.04
	0.75						0.297543	0.297728	0.06
	1.00						0.296034	0.296199	0.06
0.10	0.50	0.0	−0.5	0.1	0.5	0.2	0.299862	0.299973	0.04
		3.0					0.298176	0.298360	0.07
		5.0					0.297189	0.297327	0.05
		8.0					0.295997	0.296031	0.01
		10.0					0.295464	0.295640	0.06
0.10	0.50	1.0	−2.0	0.1	0.5	0.2	0.234668	0.234824	0.07
			−1.0				0.283758	0.283928	0.06
			0.0				0.311327	0.311564	0.08
			1.0				0.329380	0.329499	0.04
			2.0				0.343166	0.343303	0.04
0.10	0.50	1.0	−0.5	0.0	0.5	0.2	0.299063	0.299228	0.06
				0.5			0.300128	0.300340	0.07
				1.0			0.301187	0.301299	0.04
				1.5			0.302242	0.302451	0.07
				2.0			0.303291	0.303508	0.07
0.10	0.50	1.0	−0.5	0.1	0.1	0.2	0.301901	0.301896	0.00
					0.5		0.299277	0.299411	0.05
					1.0		0.296778	0.296957	0.06
					3.0		0.292024	0.292267	0.08
					5.0		0.290188	0.290425	0.08
					10.0		0.288417	0.288620	0.07
0.10	0.50	1.0	−0.5	0.1	0.5	0.0	0.316379	0.316582	0.06
						0.5	0.273271	0.273463	0.07
						1.0	0.228943	0.229040	0.04
						1.5	0.183304	0.183519	0.12
						2.0	0.136263	0.136439	0.13

The temperature profile for different values of the heat generation or absorption parameter is plotted in Fig. 2. The positive value of H_g enhances the

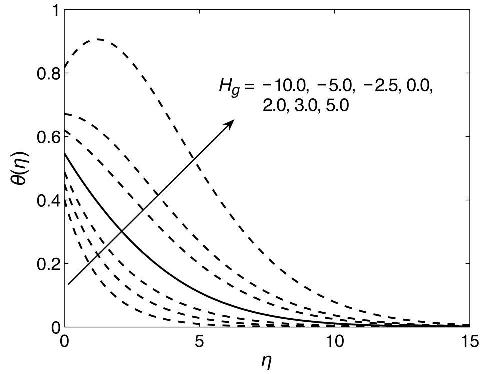

FIG. 2. Temperature profile for different values of heat generation/absorption parameter with $K = 0.1$, $\gamma = 0.5$, $\mathrm{Ri} = 1.0$, $N = -0.5$, $\mathrm{Du} = 0.1$, $\mathrm{Bi} = 0.5$, $C_r = 1.0$, and $\mathrm{Sr} = 0.2$.

thermal state of the fluid causing its temperature to increase. This is due to the fact that the thermal boundary layer is thickening. On the contrary, the negative values of H_g reduce the fluid temperature and thin the thermal boundary layer. Figure 3 shows the influence of the Dufour number on the temperature profile. Increasing the Dufour number tends to thicken the thermal boundary layer. The effect of the Biot number on the temperature profile is shown in Fig. 4. It is found that the fluid temperature is linear in the absence of the Biot number, and an increase of the Biot number, increases the fluid temperature and thermal boundary layer thickness. Figure 5 displays the effect of the chemical reaction parameter on the concentration profile. Increasing the chemical reaction parameter produces a decrease in the species concentration. In turn, this causes the concentration buoyancy effects to decrease as C_r increases. Concentration profile for different values of the Soret number is plotted in Fig. 6. It is found that the solutal boundary layer thickness increases with increasing of the Soret number.

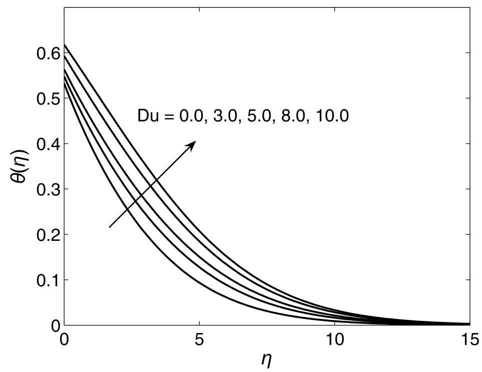

FIG. 3. Temperature profile for different values of Dufour number with $K = 0.1$, $\mathrm{Ha}^2 = 0.1$, $\gamma = 0.5$, $\mathrm{Ri} = 1.0$, $N = -0.5$, $H_g = -0.5$, $\mathrm{Bi} = 0.5$, $C_r = 1.0$, and $\mathrm{Sr} = 0.2$.

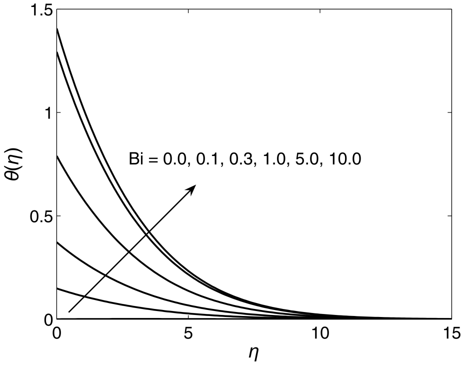

FIG. 4. Temperature profile for different values of Biot number with $K = 0.1$, $\mathrm{Ha}^2 = 0.1$, $\gamma = 0.5$, $\mathrm{Ri} = 1.0$, $N = -0.5$, $H_g = -0.5$, $\mathrm{Du} = 0.1$, $C_r = 1.0$, and $\mathrm{Sr} = 0.2$.

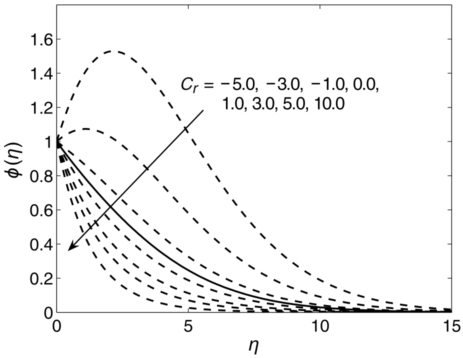

FIG. 5. Concentration profile for different values of chemical reaction parameter with $K = 0.1$, $\mathrm{Ha}^2 = 0.1$, $\gamma = 0.5$, $\mathrm{Ri} = 1.0$, $N = -0.5$, $H_g = -0.5$, $\mathrm{Du} = 0.1$, $\mathrm{Bi} = 0.5$, and $\mathrm{Sr} = 0.2$.

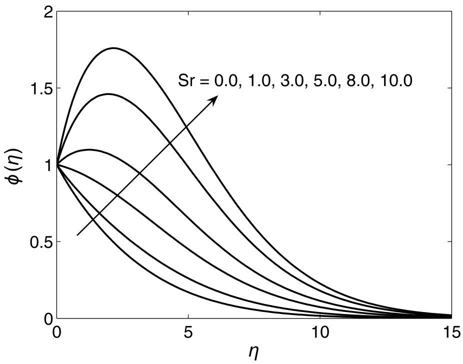

FIG. 6. Concentration profile for different values of Soret number with $K = 0.1$, $\gamma = 0.5$, $\mathrm{Ri} = 1.0$, $N = -0.5$, $\mathrm{Du} = 0.1$, $\mathrm{Bi} = 0.5$, and $C_r = 1.0$.

It is observed from Fig. 7 that the surface shear stress increases with increasing the generation/absorption parameter, Dufour number, Biot number and

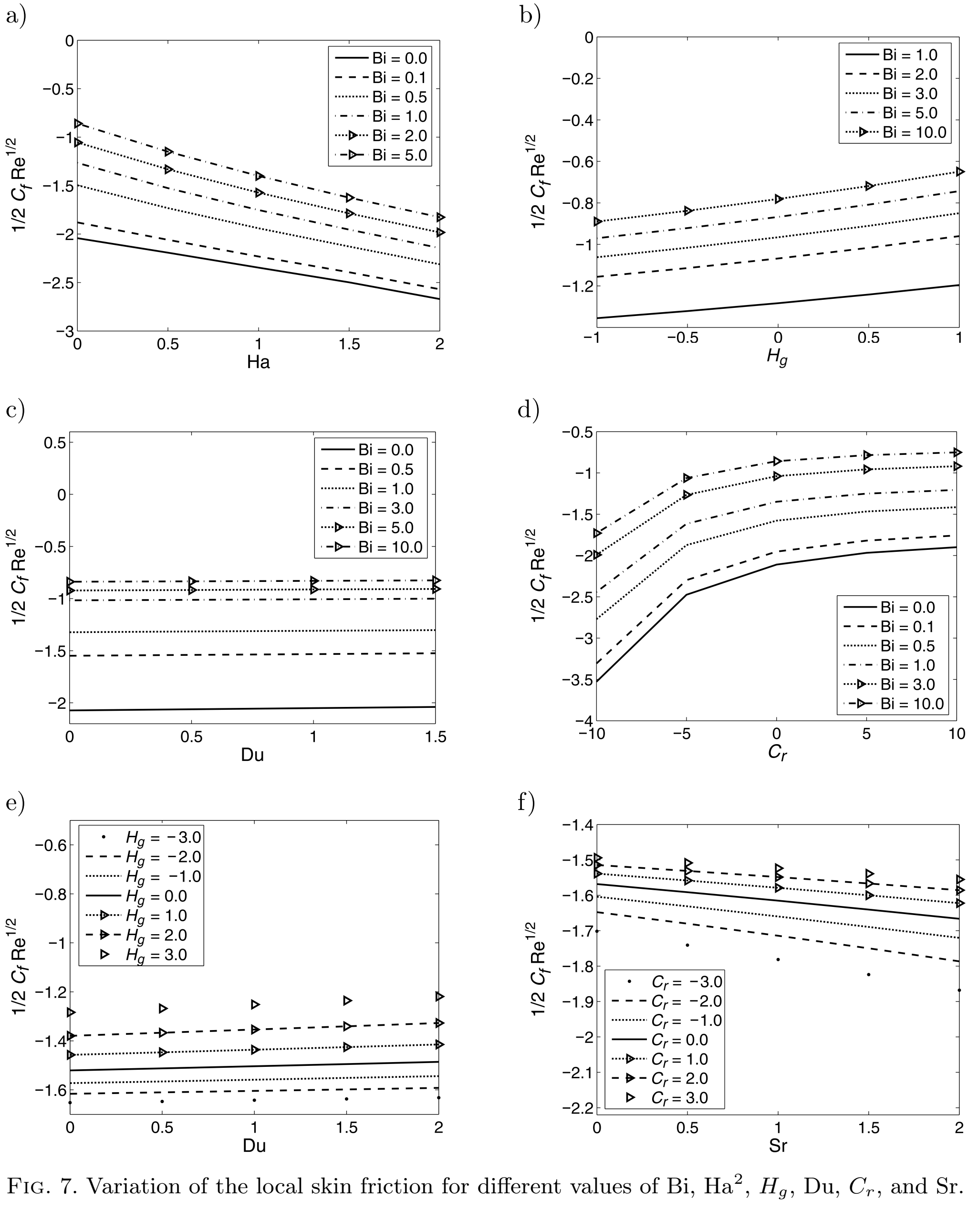

FIG. 7. Variation of the local skin friction for different values of Bi, Ha^2, H_g, Du, C_r, and Sr.

chemical reaction parameter. However, it is a decreasing function of the Hartmann number and the Soret number. In Fig. 8, it is interesting to note that the surface heat transfer rate increases with increasing the Biot number and the Soret number, and it decreases with increasing the generation/absorption parameter, Dufour number and chemical reaction parameter. It is found from the

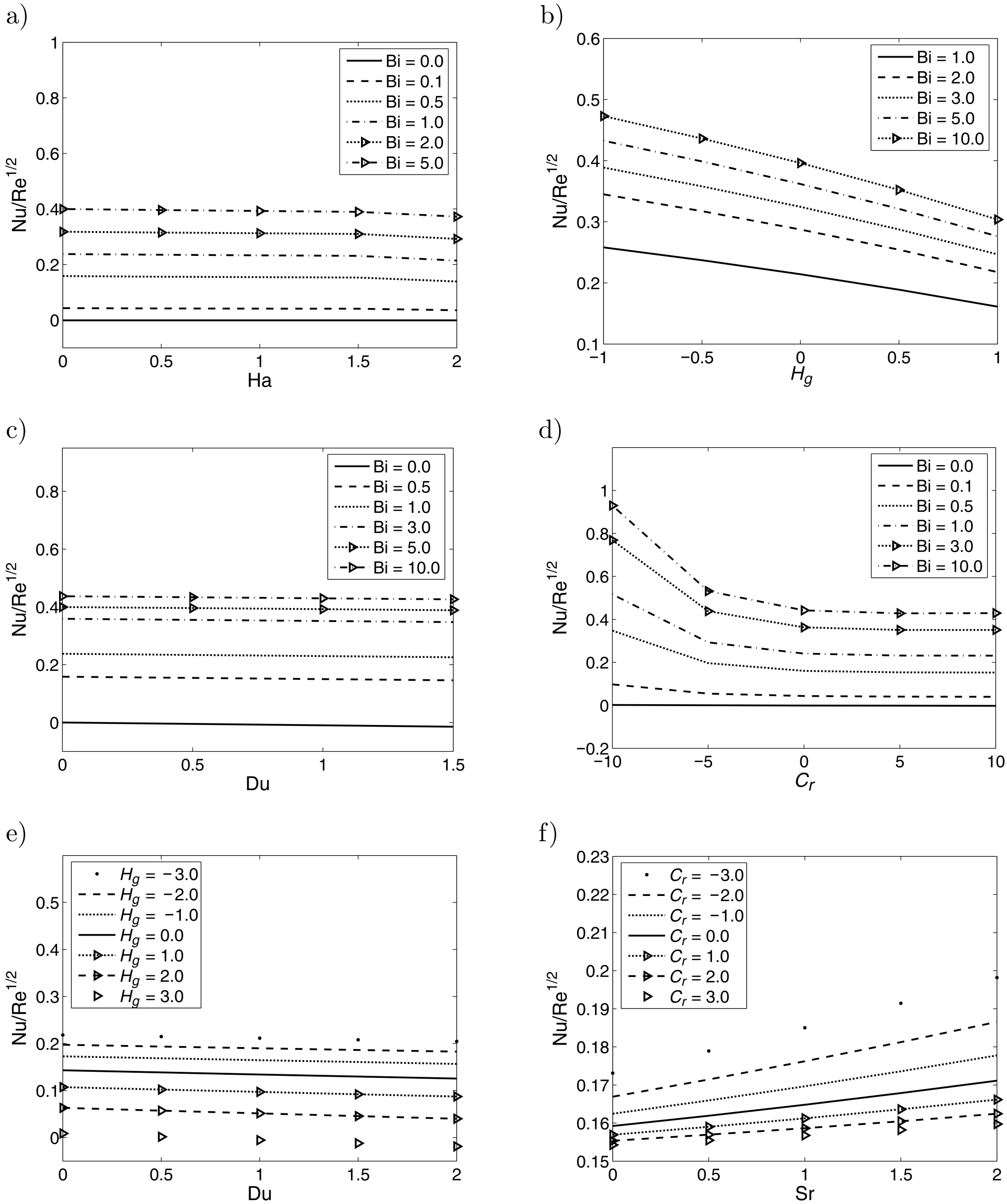

FIG. 8. Variation of the local Nusselt number for different values of Bi, Ha^2, H_g, Du, C_r, and Sr.

Fig. 9 that the surface mass transfer rate increases with increasing the generation/absorption parameter, Dufour number and chemical reaction parameter. However, the local Sherwood number decreases with increasing the Hartmann number, Biot number and Soret number.

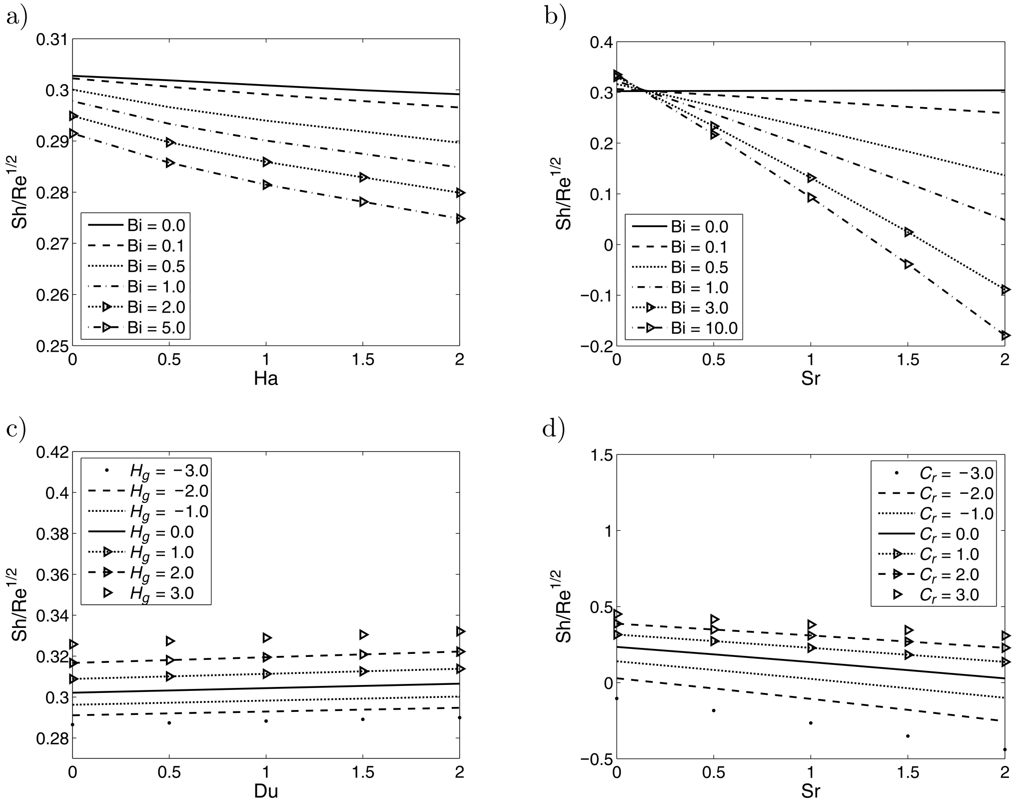

FIG. 9. Variation of the local Sherwood number for different values of Bi, Ha^2, H_g, Du, C_r, and Sr.

5. Conclusions

The present study describes the Soret and Dufour effects on mixed convection boundary layer flow over a stretching surface in a porous medium filled with viscoelastic fluid and convective boundary condition in the presence of chemical reaction and magnetic field. The governing partial differential equations are transformed into a system of non-linear ordinary differential equations by a similarity transformation. A convergent series solution is derived through the homotopy analysis method. The following are important observations:

- The thermal boundary layer thickness improves by increasing the values of heat generation or absorption parameter, Dufour number, Biot number.
- The solutal boundary layer thickness increases with increasing the Soret number and it decreases with increasing the chemical reaction parameter.
- The surface shear stress increases with increasing the heat generation or absorption parameter, Biot number, Dufour number, chemical reaction pa-

rameter and it decreases by increasing the viscoelastic parameter, Hartmann number, porosity parameter, Soret number, respectively.

- The heat transfer rate enhances with increasing the Biot number, Soret number and it decreases by increasing the porosity parameter, heat generation or absorption parameter, respectively.
- The mass transfer rate increases with increasing the viscoelastic parameter, heat generation or absorption parameter, Dufour number, chemical reaction parameter and it decreases by increasing the Hartmann number, porosity parameter, Biot number, Soret number, respectively.

References

1. Postelnicu A., I*nfluence of a magnetic field on heat and mass transfer by natural convection from vertical surfaces in porous media considering Soret and Dufour effects*, International Journal of Heat and Mass Transfer, **47**: 1467–1472, 2004.

2. Abel M.S., Mahesha N., *Heat transfer in MHD viscoelastic fluid flow over a stretching sheet with variable thermal conductivity, non-uniform heat source and radiation*, Applied Mathematical Modelling, **32**: 1965–1983, 2008.

3. Sharma B.K., Chaudhary R.C., *Hydromagnetic unsteady mixed convection and mass transfer flow past a vertical porous plate immersed in a porous medium with the Hall effect*, Engineering Transactions, **56**(1): 3–23, 2008.

4. Ahammad M.U., Mollah Md.S.H., *Numerical study of MHD free convection flow and mass transfer over a stretching sheet considering Dufour & Soret effects in the presence of magnetic field*, International Journal of Engineering and Technology, **11**(05): 4–11, 2011.

5. Chamkha A.J., Ben-Nakhi A., *MHD mixed convection-radiation interaction along a permeable surface immersed in a porous medium in the presence of Soret and Dufour's effects*, Heat Mass Transfer, **44**: 845–856, 2008.

6. Alam M.S., Rahman M.M., Samad M.A., *Dufour and Soret effects on unsteady MHD free convection and mass transfer flow past a vertical porous plate in a porous medium*, Nonlinear Analysis: Modelling and Control, **11**(3): 217–226, 2006.

7. Ibrahim W., Makinde O.D., *Magnetohydrodynamic stagnation point flow and heat transfer of Casson nanofluid past a stretching sheet with slip and convective boundary condition*, Journal of Aerospace Engineering, **29**(2): 1–11, 2016.

8. Gireesha B.J., Archana M., Prasannakumara B.C., Reddy Gorla R.S, Makinde O.D., *MHD three dimensional double diffusive flow of Casson nanofluid with buoyancy forces and nonlinear thermal radiation over a stretching surface*, International Journal of Numerical Methods for Heat and Fluid Flow, **27**(12): 2858–2878, 2017.

9. Makinde O.D., Khan W.A., Khan Z.H., *Stagnation point flow of MHD chemically reacting nanofluid over a stretching convective surface with slip and radiative heat*, Proceedings of the Institution of Mechanical Engineers, Part E: Journal of Process Mechanical Engineering, **231**(4): 695–703, 2017.

10. Makinde O.D., Mishra S.R., *Chemically reacting MHD mixed convection variable viscosity Blasius flow embedded in a porous medium*, Defect and Diffusion Forum, **374**: 83–91, 2017.

11. Sharma P.R., Choudhary S., Makinde O.D., *MHD slip flow and heat transfer over an exponentially stretching permeable sheet embedded in a porous medium with heat source*, Frontiers in Heat and Mass Transfer, **9**: 1–7, 2017.

12. Sreedevi G., Prasada Rao D.R.V., Makinde O.D., Ramana Reddy G.V., *Soret and Dufour effects on MHD flow with heat and mass transfer past a permeable stretching sheet in presence of thermal radiation*, Indian Journal of Pure and Applied Physics, **55**: 551–563, 2017.

13. Bhuvaneswari M., Sivasankaran S., Ferdows M., *Lie group analysis of natural convection heat and mass transfer in an inclined surface with chemical reaction*, Nonlinear Analysis: Hybrid System, **3**: 536–542, 2009.

14. Chamkha A.J., Ahmed S.E., *Similarity solution for unsteady MHD flow near a stagnation point of a three-dimensional porous body with heat and mass transfer, heat generation/absorption and chemical reaction*, Journal of Applied Fluid Mechanics, **4**: 87–94, 2011.

15. Karthikeyan S., Bhuvaneswari M., Sivasankaran S., Rajan S., *Soret and Dufour effects on MHD mixed convection heat and mass transfer of a stagnation point flow towards a vertical plate in a porous medium with chemical reaction, radiation and heat generation*, Journal of Applied Fluid Mechanics, **9**: 1447–1455, 2016.

16. Kasmani M., Sivasankaran S., Bhuvaneswari M., Siri Z., *Effect of chemical reaction on convective heat transfer of boundary layer flow in nanofluid over a wedge with heat generation/absorption and suction*, Journal of Applied Fluid Mechanics, **9**: 379–388, 2016.

17. Makinde O.D., Aziz A., *MHD mixed convection from a vertical plate embedded in a porous medium with convective boundary condition*, International Journal of Thermal Sciences, **49**: 1813–1820, 2010.

18. Subhashini S.V., Samuel N., Pop I., *Double-diffusive convection from a permeable vertical surface under convective boundary condition*, International Communications in Heat and Mass Transfer, **38**: 1183–1188, 2011.

19. Abdelkhalek M.M., *Heat and mass transfer in MHD flow from a permeable surface with heat generation effects*, Engineering Transactions, **56**(4): 325–344, 2008.

20. Yao S., Fang T., Zhong Y., *Heat transfer of a generalized stretching/shrinking wall problem with convective boundary conditions*, Communications in Nonlinear Science and Numerical Simulation, **16**: 752–760, 2011.

21. Eswaramoorthi S., Bhuvaneswari M., Sivasankaran S., Rajan S., *Effect of radiation on MHD convective flow and heat transfer of a viscoelastic fluid over a stretching surface*, Procedia Engineering, **127**: 916–923, 2015.

22. Eswaramoorthi S., Bhuvaneswari M., Sivasankaran S., Rajan S., *Soret and Dufour effects on viscoelastic boundary layer flow over a stretching surface with convective*

boundary condition with radiation and chemical reaction, Scientia Iranica, **23**(6): 2575–2586, 2016.

23. Hayat T., Mustafa M., Pop I., *Heat and mass transfer for Soret and Dufour's effect on mixed convection boundary layer flow over a stretching vertical surface in a porous medium filled with a viscoelastic fluid*, Communications in Nonlinear Science and Numerical Simulation, **15**: 1183–1196, 2010.

Received May 17, 2017; accepted version November 29, 2018.